Identification and Structural Mechanism for a Novel Interaction between a Ubiquitin Ligase WWP1 and Nogo-A, a Key Inhibitor for Central Nervous System Regeneration[†,‡]

Haina Qin,[§] Helen X. Pu,[||] Minfen Li,[§] Sohail Ahmed,[||] and Jianxing Song*[,§,⊥]

Department of Biological Sciences, Faculty of Science, National University of Singapore, Singapore, Neural Stem Cell Laboratory, 61, Biopolis Drive, Proteos Building, Singapore 138673, and Department of Biochemistry, Yong Loo Lin School of Medicine, National University of Singapore, Singapore

Received September 21, 2008; Revised Manuscript Received November 7, 2008

ABSTRACT: Nogo-A has been extensively demonstrated to play key roles in inhibiting central nervous system regeneration, regulating endoplasmic reticulum formation, and maintaining the integrity of the neuromuscular junction. In this study, an E3 ubiquitin ligase WWP1 was first identified to be a novel interacting partner for Nogo-A both in vitro and in vivo. By using CD, ITC, and NMR, we have further conducted extensive studies on all four WWP1 WW domains and their interactions with a Nogo-A peptide carrying the only PPxY motif. The results lead to several striking findings. (1) Despite containing an unstructured region, the 186-residue WWP1 fragment containing all four WW domains is able to interact with the Nogo-A(650−666) peptide with a high affinity, with a dissociation constant (K_d) of 1.68 μM. (2) Interestingly, four isolated WW domains show differential structural properties in the free states. WW1 and WW2 are only partially folded, while WW4 is well-folded. Nevertheless, they all become well-folded upon binding to Nogo-A(650−666), with K_d values ranging from 1.03 to 3.85 μM. (3) The solution structure of the best-folded WW4 domain is determined, and the binding-perturbed residues were derived for both WW4 and Nogo-A(650−666) by NMR HSQC titrations. Moreover, on the basis of the NMR data, the complex model is constructed by HADDOCK 2.0. This study provides rationales as well as a template Nogo-A(650−666) for further design of molecules to intervene in the WWP1−Nogo-A interaction which may regulate the Nogo-A protein level by controlling its ubiquitination.

Nogo is a member of the reticulon (RTN) family of proteins named after their main subcellular localization in the endoplasmic reticulum (ER). Three major protein variants (Nogo-A, -B, and -C) are derived from the Nogo gene by both alternative splicing and promoter use (*1, 2*). Among them, the 1192-residue Nogo-A (human) is the largest and has attracted intense research in recent years because of its role in the inhibition of CNS[1] regeneration. Nogo-A has been demonstrated to be a potent neurite growth inhibitor and plays a key role both in the restriction of axonal regeneration after injury and in the structural plasticity of the CNS of higher vertebrates (*3*−*8*). In vivo neutralizing Nogo-A by its antibody has been shown to enhance sprouting and functional recovery after cervical lesion in rat (*9*) and adult primates (*10*). In addition, Nogo-A was also identified to be essential for the tubular network formation of ER (*11*). Most recently, a role of Nogo-A in synapse integrity has also been suggested, and overexpression of Nogo-A led to destabilization and retraction of nerve termini (*12*).

So far, three distinct regions of Nogo-A were shown to be important for its known functions (*7*): (1) an N-terminal region (amino acids 1−172) involved in the inhibition of fibroblast spreading, (2) a stretch (amino acids 544−725) encoded by the Nogo-A-specific exon that restricts neurite outgrowth and cell spreading and induces growth cone collapse, and (3) a C-terminal region (Nogo-66) with growth cone collapsing function. The segment spanning residues 544−725 displays the most potent inhibitory effect. In addition, it has been proposed that the two Cys residues (at positions 575 and 676) within the Nogo-A-specific region are very important for shaping of ER as well as ER tubule formation (*11*).

[†] This study was supported by Ministry of Education (MOE) Tier 2 Grant R-154-000-388-112 to J.S.

[‡] The structural coordinates of the WWP1 WW4 domain were deposited in the Protein Data Bank as entry 2OP7, and NMR data were deposited in RCSB as entry RCSB041415.

* To whom correspondence should be addressed. Phone: (65) 6516-1013. Fax: (65) 6779-2486. E-mail: bchsj@nus.edu.sg.

[§] Faculty of Science, National University of Singapore.

[||] Neural Stem Cell Laboratory.

[⊥] Yong Loo Lin School of Medicine, National University of Singapore.

[1] Abbreviations: CNS, central nervous system; WWP1, WW domain containing E3 ubiquitin protein ligase 1; MAG, myelin-associated glycoprotein; OMgp, oligodendrocyte myelin glycoprotein; GST, glutathione *S*-transferase; IPTG, isopropyl β-D-1-thiogalactopyranoside; EDTA, ethylenediaminetetraacetic acid; SDS−-PAGE, sodium dodecyl sulfate−polyacrylamide gel electrophoresis; PVDF, polyvinylidene fluoride; CD, circular dichroism; ITC, isothermal titration calorimetry; HADDOCK, High Ambiguity Driven protein−protein Docking; HPLC, high-performance liquid chromatography; NMR, nuclear magnetic resonance; HSQC, heteronuclear single-quantum correlation; TOCSY, total correlation spectroscopy; NOESY, nuclear Overhauser enhancement spectroscopy; COSY, correlation spectroscopy; NOE, nuclear Overhauser effect.

10.1021/bi8017976 CCC: $40.75
Published on Web 11/26/2008

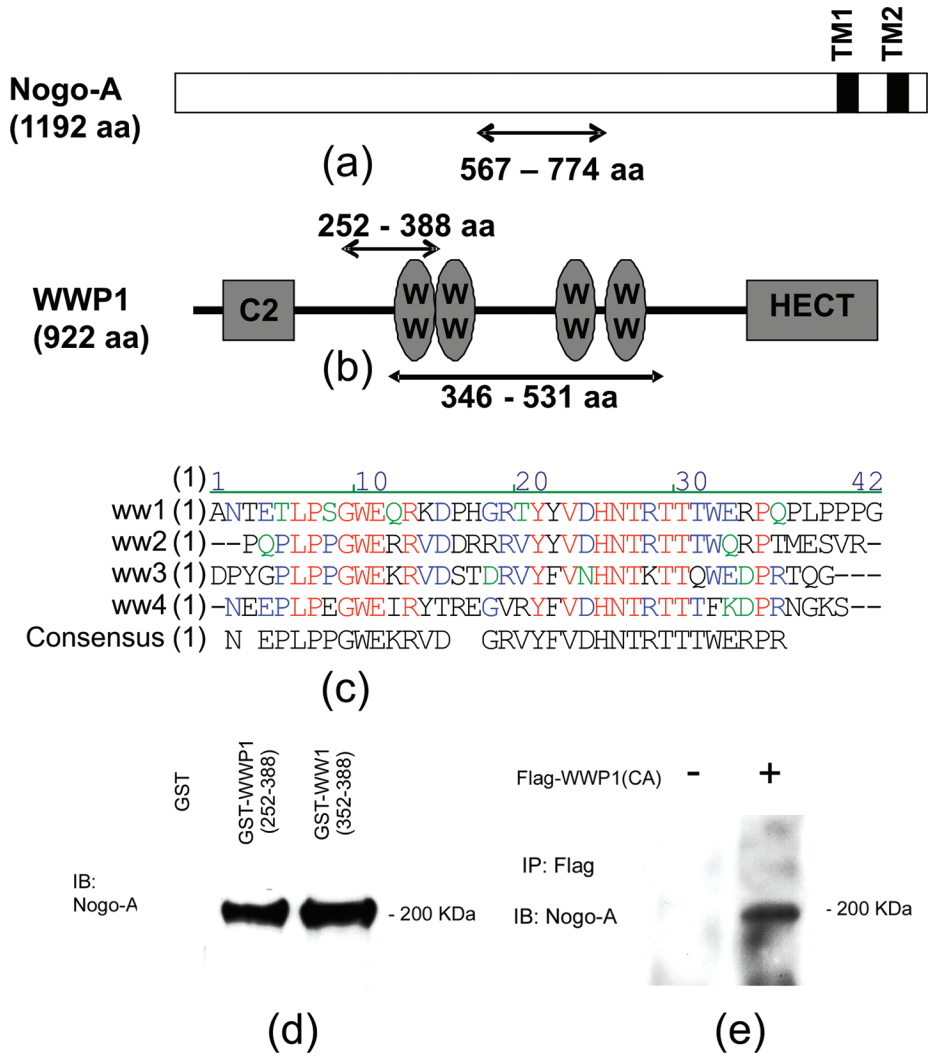

FIGURE 1: Identification of the novel binding of WWP1 to Nogo-A. (a) Schematic representation of the human Nogo-A protein, with the fragment used as the bait indicated. (b) Schematic representation of the human WWP1 protein, with two fragments used for the pull-down experiments indicated. (c) Sequence alignment of the four human WWP1 WW domains. (d) Pull-down of endogenous Nogo-A in N1E115 cells by the GST-fused WWP1(252−388) fragment and GST-fused WW1(352−388) but not by GST alone. (e) Co-immunoprecipitation of WWP1 with endogenous Nogo-A. N1E115 cells were transfected with Flag-tagged mutant WWP1 (C890A). Cell lysates were incubated with anti-Flag antibody, and the immunoprecipitates were analyzed with anti-Nogo-A antibody.

Because of its multifunctional nature, Nogo-A has been thought to have the capacity to interact with many different protein partners. However, so far, only NgR was functionally validated to be the receptor for Nogo-66 (*13*), a C-terminal extracellular loop highly conserved among all three Nogo members which adopts an unusual helical structure (*14, 15*). NgR is also found to interact with other myelin-associated proteins such as MAG and OMgp (*16*). Therefore, it is of significant interest to identify new interacting molecules (receptors or intracellular binding partners) engaged in Nogo-A processing and signaling.

Previously, we have systematically mapped out the structural properties of all three Nogo variants (*14, 15, 17*), as well as identified a novel interaction between Nogo-A and Nck2 (*18*). In this study, we used one human Nogo-A-specific fragment over residues 567−774 (Figure 1a) previously constructed (*17*) as a bait for screening its binding partner from the human cDNA library displayed on T7 phage capsids. This led to the identification of WWP1, an E3 ubiquitin ligase (Figure 1b), as a novel binding partner of Nogo-A. Both proteins were further demonstrated to be physiologically associated in vivo by immunoprecipitation. Consequently, we further conducted extensive characterizations of all four WWP1 WW domains, as well as their interactions with Nogo-A by use of circular dichroism (CD), isothermal titration calorimetry (ITC), and NMR spectroscopy.

MATERIALS AND METHODS

T7 Phage Library Screening. An aliquot of a T7 phage display library of human brain cDNA (Novagen) was precleared with 100 μg of GST protein immobilized on glutathione-Sepharose beads (Amersham Biosciences) by incubating them together for 2 h at room temperature. The supernatant was then incubated overnight at 4 °C with 100 μg of GST-fused Nogo-A(567−774) immobilized on glutathione-Sepharose beads. All binding experiments were performed in the presence of 1% bovine serum albumin. Unbound phages were washed four times with TBST [0.1% Tween in 10 mM Tris (pH 7.4) and 150 mM NaCl]. The bound phages were amplified in *Escherichia coli* BL5615 (Novagen) which was preinduced with 1 mM IPTG for 20 min at 37 °C. After cell lysis, the phage lysate was clarified by centrifugation at 8000*g* for 10 min and stored at 4 °C for

use in the next selection round. Five rounds of selection were carried out in total. PCR analysis was performed on amplified phages using a pair of T7 primers to ascertain the enrichment. Plaque assays were again used to confirm the binding of selected phage clone with the bait. A pool of phages from a single phage clone was plated, and the plaques were transferred to a hydro bond C membrane. The membrane was then incubated with the GST-fused Nogo-A-specific fragment (2 μg/mL) overnight at 4 °C. After four washes with PBST (0.1% Tween in PBS), the binding between phage-displayed protein and the GST-fused Nogo-A-specific fragment was detected by the anti-GST antibody followed by alkaline phasphatase (AP)-conjugated secondary antibody.

GST Pull-Down Assays. N1E115 cells were lysed in NP-40 lysis buffer [1% Nonidet P-40, 20 mM Tris-HCl (pH 7.5), 150 mM NaCl, 5 mM EDTA, and protease inhibitors from Roche] for 10 min at 4 °C, and insoluble materials were removed by centrifugation at 15000*g* and 4 °C for 10 min. GST fusion proteins (5 μg) of the WWP1 fragments (amino acids 252−388) and (amino acids 352−388) containing only the first WW domain (Figure 1b) were added to cell lysates generated from $\sim 1 \times 10^7$ cells and incubated for 2 h at 4 °C, followed by addition of 50 μL of glutathione-Sepharose beads for 1 h. Precipitates were washed four times with NP-40 lysis buffer and subjected to SDS−PAGE (8%) and immunoblotting with anti-Nogo-A antibody.

In Vivo Immunoprecipitation. Mouse N1E115 neuroblastoma cells and Mouse NIH3T3 cells were grown in Dulbecco's modified Eagle's medium with high glucose (Invitrogen) supplemented with 10% fetal bovine serum at 5% CO_2. The transfections of plasmids (range of 3−10 μg) on N1E115 cells were carried out with lipofectAMINE2000 transfection reagent (Invitrogen) according to the manufacturer's protocol.

Cell lysates were incubated with antibodies (1 μg) overnight at 4 °C, followed by addition of 50 mL of protein A/G Plus-Sepharose beads (Santa Cruz Biotechnology) for an additional 2 h at 4 °C. Immunoprecipitates were washed four times with Nonidet P-40 lysis buffer and boiled in 30 mL of 2× Laemmli buffer. Samples were subjected to 6 or 8% SDS−polyacrylamide gel electrophoresis (PAGE) analysis and electrotransferred onto PVDF membranes. Membranes were probed with the indicated primary antibodies, followed by horseradish peroxidase-conjugated secondary antibodies. Membranes were then washed and visualized with an enhanced chemiluminescence (ECL) detection system (Amersham Pharmacia Biotech). When necessary, membranes were stripped by incubation in 62.5 mM Tris-HCl (pH 6.7), 100 mM 2-mercaptoethanol, and 2% SDS for 1 h at 50 °C with constant agitation, washed, and then reprobed with other antibodies as indicated.

Cloning and Generation of Various Recombinant Proteins and/or Peptides. DNA fragments encoding different WWP1 and Nogo-A regions were obtained by amplification PCRs. Subsequently, the DNA fragment encoding the protein containing all four WW domains (corresponding to WWP1 residues 346−531 and designated as fWW) was cloned into vector pET32a (Novagen) as previously described (*18*), while the others were cloned into vector pGEX-4T1 (Pharmacia Biotech), which include those encoding four isolated WW domains designated WW1, WW2, WW3, and WW4 (corresponding to WWP1 residues 346−385, 380−417, 453−491, and 494−531, respectively), as well as the Nogo-A(650−666) peptide with a sequence of KHEPENPPPYEEAMSVS. Constructs containing Flag-WWP1 were kindly provided by Dr. Miyazawa from the University of Tokyo (Tokyo, Japan) (*19*).

For bacterial expression of the recombinant proteins, the vectors were transformed into *E. coli* BL21 cells. The cells were then cultured at 37 °C until the OD_{600} value reached 0.6. Subsequently, IPTG was added into the broth to a final concentration of 0.3 mM to induce protein expression for 12 h at 20 °C. Cells were harvested by centrifugation and lysed by sonication in PBS buffer. The recombinant GST-fused WW1−4 proteins and Nogo-A peptide were purified by affinity chromatography with glutathione-Sepharose 4B beads (Pharmacia Biotech) under native conditions. Four individual WW domains and Nogo-A(650−666) were released from their GST fusion proteins by on-gel thrombin cleavage at room temperature for 3 h. The released WW domains and Nogo-A(650−666) peptide were further purified by HPLC on a reverse-phase C_{18} column (Vydac). The fWW protein was overexpressed in *E. coli* BL21 cells but found in the inclusion body. Consequently, it was purified with Ni-NTA agrose (QIAGEN) under denaturing conditions followed by a further HPLC purification on a reverse-phase C_4 column (Vydac). To isotope label fWW, WW1−4 proteins, and Nogo-A(650−666) required for heteronuclear NMR experiments, recombinant proteins were prepared with a similar protocol except the cells were grown in M9 medium with addition of $(^{15}NH_4)_2SO_4$ for ^{15}N labeling and $(^{15}NH_4)_2SO_4$/[^{13}C]glucose for double labeling, respectively (*20*).

CD, NMR Sample Preparation, and Characterization. CD and NMR samples were prepared by dissolving proteins or peptides in 5 mM phosphate buffer (pH 6.2). For NMR samples, 10% D_2O was additionally added for spin lock.

CD experiments were performed on a Jasco J-810 spectropolarimeter equipped with a thermal controller as described previously (*18*). The far-UV CD spectra of the fWW and WW1−4 domains were collected at a protein concentration of $\sim$20 μM at 25 °C, using a 1 mm path length cuvette with a 0.1 nm spectral resolution. Data from three independent scans were added and averaged.

All NMR experiments were conducted on an 800 MHz Bruker Avance spectrometer equipped with pulse field gradient units at 25 °C as previously described (*18, 20*−*22*). The NMR spectra acquired for both backbone and side chain assignments included HNCACB, CBCA(CO)NH, ^{13}C-edited H(CCC)-TOCSY, NOESY, $^1H-^{15}N$ HSQC, ^{15}N-edited HSQC-TOCSY, and HSQC-NOESY. For structural determination, two-dimensional ^1H TOCSY spectra, NOESY spectra in D_2O, and DQF-COSY spectra in H_2O were acquired to extract NOE distance and dihedral angle constraints. NMR data were processed with NMRpipe (*23*) and analyzed with NMRview (*24*).

Isothermal Titration Calorimetry (ITC) Characterization. All isothermal titration calorimetric (ITC) experiments were performed using a Microcal VP ITC machine as previously described (*18, 20*). Titrations of the binding of fWW and WW1−4 to the Nogo-A(650−666) peptide were conducted in the same buffer [5 mM phosphate buffer (pH 6.2)] and at the same temperature (25 °C). The fWW and WW1−4 samples were placed in a 1.8 mL sample cell, while the Nogo-A(650−666) sample was loaded into a 300 μL syringe.

The samples were degassed for 15 min to remove bubbles before titrations were initiated. A control experiment with the same parameter setting was also performed to subtract the contribution of the peptide dilution. The titration data after the results of the control experiment had been subtracted were fitted using the built-in software ORIGIN to yield the thermodynamic binding parameters listed in Table 1.

NMR Characterization of Binding. To NMR characterize the binding of the Nogo-A(650−666) peptide to fWW or WW1−4, two-dimensional $^{1}H-^{15}N$ HSQC spectra of the ^{15}N-labeled WW domains were acquired at a protein concentration of ~100 μM in the absence or presence of Nogo-A(650−666) at different molar ratios. By superimposing the HSQC spectra of the ^{15}N-labeled WW domains in the absence and presence of Nogo-A(650−666), we could identify the shifted HSQC peaks as previously described (*18, 25*). Similarly, the binding interactions were also assessed by monitoring HSQC peak shifts of the ^{15}N-labeled Nogo-A(650−666) peptide. Similarly, the binding-perturbed peaks were mapped out by superimposing the HSQC spectra of the ^{15}N-labeled Nogo-A(650−666) peptide in the absence and presence of the WW domains. The degree of binding-induced chemical shift difference (CSD) was represented by an integrated chemical shift index calculated by the formula $[(\Delta^{1}H)^2 + (\Delta^{15}N/4)^2]^{1/2}$ ppm (*18, 25*).

NMR Structure of the WW4 Domains in the Free and Complexed States. To determine the three-dimensional structure of the best-structured WW4 domain, a set of unambiguous NOE restraints extracted from three-dimensional ^{15}N HSQC-NOESY and two-dimensional ^{1}H NOESY spectra were input to calculate initial structures with CYANA (*26*) together with dihedral angle restraints derived from $^{3}J_{\alpha HN-NH}$ coupling constants from a two-dimensional DQF-COSY spectrum as well as predicted by TALOS on the basis of chemical shift values (*27*). With the availability of the initial structure, more NOE cross-peaks in the two NOESY spectra were assigned with the assistance of CYANA followed by a manual confirmation. The 10 structures with lowest target functions accepted by CYANA were selected and assessed by PROCHECK (*28*) and subsequently analyzed by using MolMol (*29*) and Pymol (http://www.pymol.org). The structural statistics are presented in Table 2. The structural coordinates of the WWP1 WW4 domain was deposited in the Protein Data Bank as entry 2OP7, and NMR data were deposited with the RCSB as entry RCSB041415.

The model of the WW4 domain in complex with the Nogo-A peptide was constructed by the computational docking with the well-established program HADDOCK2.0 (High Ambiguity Driven protein−protein Docking), which makes use of chemical shift perturbation data to drive the docking while allowing various degrees of flexibility (*25, 30*). The docking procedure was performed in three steps: (1) randomization and rigid body energy minimization, (2) semiflexible simulated annealing, and (3) flexible explicit solvent refinement. To avoid being trapped, Nogo-A(650−666) segments K650-H651 and A662-M663-S664-V665-S666 that showed no detectable shift in the HSQC titration were not included in molecular docking. Consequently, according to the HADDOCK definition, the accessible residues with large chemical shift difference (CSD) values were set as active residues, which include Trp9−Ile11, Tyr20−Lys32 of the WW4 domain, and Glu652−Glu661 of Nogo-A.

Table 1: Thermodynamic Parameters of the Binding Interactions of the Nogo-A(650−666) Peptide with fWW and Four Individual WW Domains

syringe	cell	buffer	volume of each injection (μL)	K_a (M^{-1})	K_d (μM)	stoichiometry (n)	ΔS (cal mol^{-1} K^{-1})	ΔH (cal/mol)
Nogo-A(650−666) (0.5 mM)	fWW (0.005 mM)	phosphate (5 mM, pH 6.2)	5	$5.938 \times 10^5 \pm 6.823 \times 10^4$	1.68	4.000 ± 0	23.08	−994 ± 17.78
Nogo-A(650−666) (0.2 mM)	WW1 (0.01 mM)	phosphate (5 mM, pH 6.2)	5	$9.70 \times 10^5 \pm 4.5 \times 10^4$	1.03	1.07 ± 0	−222	$-7.434 \times 10^4 \pm 555$
Nogo-A(650−666) (0.16 mM)	WW2 (0.005 mM)	phosphate (5 mM, pH 6.2)	5	$2.60 \times 10^5 \pm 1.6 \times 10^4$	3.85	0.9 ± 0	−29.3	$-1.613 \times 10^4 \pm 383$
Nogo-A(650−666) (0.16 mM)	WW3 (0.005 mM)	phosphate (5 mM, pH 6.2)	5	$5.41 \times 10^5 \pm 6.5 \times 10^4$	1.85	0.95 ± 0	−54.2	$-2.399 \times 10^4 \pm 809$
Nogo-A(650−666) (0.16 mM)	WW4 (0.007 mM)	phosphate (5 mM, pH 6.2)	5	$6.68 \times 10^5 \pm 2.7 \times 10^4$	1.50	0.942 ± 0.0076	−57.7	$-2.514 \times 10^4 \pm 331$

Table 2: Structural Statistics for the 10 Selected NMR Structures of the WWP1 WW4 Domain

experimental constraints for structure calculation	
no. of NOE restraints	
total	263
intraresidue	119
sequential	49
medium-range	17
long-range	78
no. of dihedral angle constraints	
total	54
ϕ	29
ψ	25
CYANA target function	0.63 ± 0.035
no. of distance violations of >0.20 Å	0
no. of dihedral angle violations of >5°	0
Ramachandran statistics (%)	
most favored	71.0
additionally allowed	22.6
generously allowed	6.5
disallowed	0.0
root-mean-square deviation (Å) (secondary structure regions)	
all atoms	1.37
heavy atoms	1.12
backbone atoms	0.25

Initially, 1000 structures were generated in the rigid body docking, and subsequently, the 100 best structures were selected for further semiflexible simulated annealing. Only the 20 best structures were subjected to the final refinement in explicit water. On the basis of the overall HADDOCK score, the best structural solution was selected for detailed analysis and display.

RESULTS

Identification of WWP1 as a Novel Binding Partner for Nogo-A. A Nogo-A-specific fragment (residues 567−774) was fused to GST and used as the bait in a phage display screening (*31, 32*). The screening was performed on a human brain cDNA library displayed by a T7 phage vector for five rounds of affinity selection. The enrichment after each round of selection was analyzed by performing PCR using T7 primers. A single PCR product was clearly emerging after a third round of selection. The phage display of this specific protein becomes dominant in the fourth and fifth selection. Sequencing of this PCR product revealed that this cDNA encoded a WWP1 fragment containing residues 252−388.

Examination of the WWP1 fragment selected from phage screening revealed that it contained the first WW domain, which has been extensively documented to bind the proline-rich consensus sequences with the motif PPxY. Indeed, the Nogo-A(567−774) fragment used as the bait in this experiment did contain a PPPY motif (residues 656−659) which is the only PPxY motif in the complete Nogo-A sequence. In this regard, it is highly likely that the WWP1 and Nogo-A proteins interact with each other through binding between WW domains and the PPPY motif. To verify this, we mutated Tyr659 to Ala in the GST-fused Nogo-A(567−774) peptide. A plaque assay again was used to assess the binding between mutated Nogo-A(567−774) (Y/A) and WWP1 fragment. Strikingly, the result indicated that the binding was completely abolished by the Tyr659 to Ala mutation.

WWP1 Interacts with Nogo-A in Vivo. N1E115 neuroblastoma cells were used to detect whether WWP1 was indeed associated with the endogenous Nogo-A. The binding interaction was first assessed by a GST pull-down assay using the GST-WWP1 fragment (residues 252−388) and GST-WW1 domain (residues 352−388). More specifically, lysates of N1E115 cells were incubated with the respective GST proteins, and the precipitates were then analyzed with anti-Nogo-A antibodies. As seen in Figure 1d, both the GST-WWP1 fragment (residues 252−388) and the GST-WW1 domain (residues 352−388) were able to pull down the endogenous Nogo-A from N1E115 cells.

The immunoprecipitation was further performed to examine whether WWP1 and Nogo-A were physiologically associated in vivo. The Flag-tagged WWP1 (C890A with the well-established catalytic Cys at residue 890 replaced with an Ala) was transfected into N1E115 cells. The rationale for using this mutated construct is to prevent the degradation of Nogo-A mediated by WWP1 and thus to facilitate detection of the interaction. As shown in Figure 1e, the immunoprecipitation (IP) of Flag-tagged WWP1 (CA) resulted in co-IP of Nogo-A which was subsequently detected with the anti-Nogo-A antibody. This result clearly indicates that Nogo-A is indeed physiologically associated with WWP1.

Preliminary CD and NMR Characterization. The in vitro and in vivo experiments described above have clearly demonstrated that the first WW domain in the WWP1 fragment interacted with the PPPY motif in the Nogo-A fragment. However, as seen in Figure 1b, WWP1 contains four WW domains over residues 346−531, with a ~40-residue linker between the second and third WW domains. To study the structural properties and assess whether all four WW domains are capable of interacting with the PPPY motif in the Nogo-A fragment, we have cloned the His-tagged WWP1 fragment containing all four WW domains (fWW) over residues 346−531, as well as the four individual WW domains (WW1−4), as GST fusion proteins with their sequences shown in Figure 1c. On the other hand, we also cloned and expressed the Nogo-A(650−666) peptide containing the only PPxY motif of Nogo-A for the binding study.

The fWW recombinant protein was overexpressed but presented in the inclusion body. Consequently, it was obtained by Ni^{2+}-agarose affinity column purification under denaturing conditions followed by HPLC purification on a reverse-phase C_4 column. On the other hand, the recombinant proteins of four individual WW domains and the Nogo-A(650−666) peptide were released by the in-gel thrombin cleavage of the GST fusion proteins followed by HPLC purification on a reverse-phase C_{18} column.

The structural property of the fWW protein was first assessed by far-UV CD spectroscopy. As seen in Figure 2a, the protein had a far-UV CD spectrum with a positive signal at ~230 nm and a maximal negative signal at ~205 nm, but without any positive signal below 200 nm. This observation implies that the fWW protein consists of the β-turn secondary structure, together with some random coil (*33, 34*).

We have prepared ^{15}N isotope-labeled fWW protein and subsequently acquired its $^{1}H-^{15}N$ HSQC spectrum. The fWW protein had a relatively dispersed HSQC spectrum, with some peaks even located at ~9.5 ppm (Figure 2b). However, only ~80 resonance peaks could be detected in the spectrum, much fewer than its number of residues (186). In particular, of these peaks, ~40 had very strong intensities

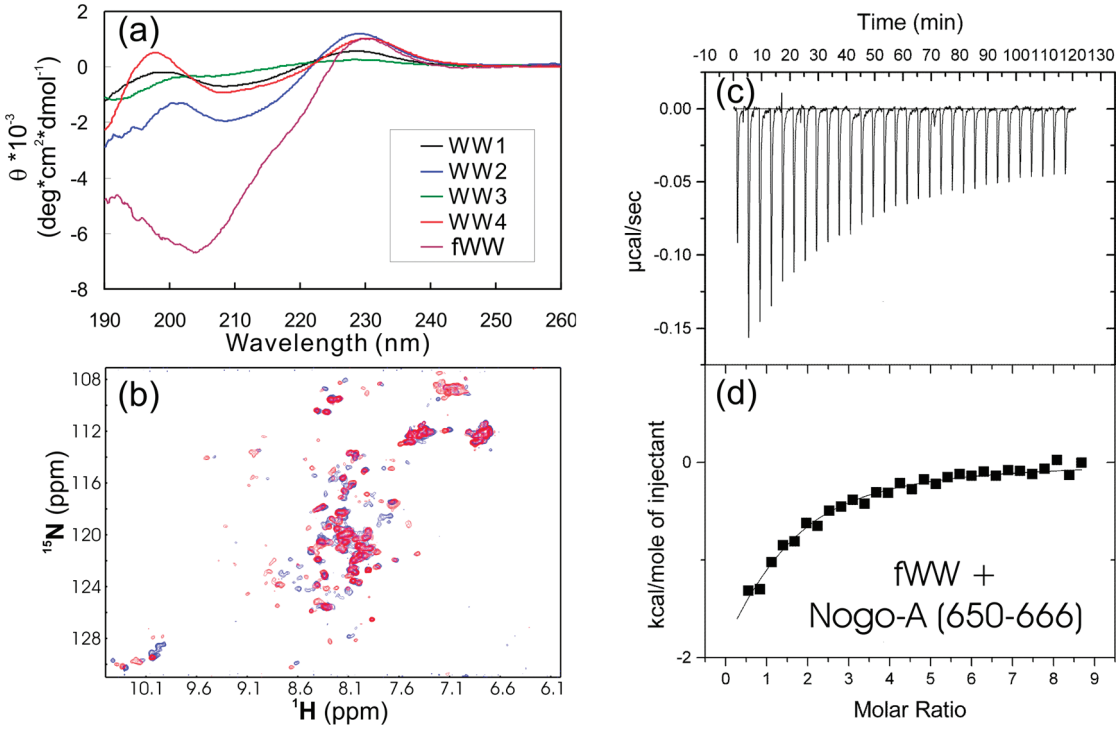

FIGURE 2: Structural and binding characterization of the fWW protein. (a) Far-UV CD spectra of fWW and four isolated WW domains at protein concentrations of ~20 μM in 5 mM phosphate buffer (pH 6.2) at 25 °C. (b) Superimposition of the HSQC spectra of the ^{15}N-labeled fWW protein in the absence (blue) and presence (red) of Nogo-A(650−666) at a molar ratio of 1:4 (fWW:peptide). Spectra were acquired in 5 mM phosphate buffer (pH 6.2) at 25 °C on an 800 MHz Bruker NMR spectrometer. (c) ITC titration profiles of the binding reaction of the fWW protein with Nogo-A(650−666). (d) Integrated values for reaction heats with subtraction of the corresponding blank results normalized by the amount of ligand injected vs the Nogo-A:fWW molar ratio. The detailed conditions and setting of the ITC experiments are presented in Materials and Methods as well as Table 1.

while the rest had much weaker intensities. This observation implies that the strong HSQC peaks may result from the ~40-residue linker region between the second and third WW domains which might be highly unstructured. Nevertheless, as seen in Figure 2b, upon addition of the Nogo-A(650−666) peptide, many HSQC peaks of the fWW protein shifted significantly, indicating that it was able to interact with Nogo-A. Unfortunately, due to the very limited manifestation of the HSQC peaks as well as a strong tendency to aggregate at a high concentration, detailed NMR study is not feasible for the fWW protein. However, as presented in panels c and d of Figure 2 and Table 1, the thermodynamic parameters for the binding of fWW to the Nogo-A peptide were successfully obtained by using the ITC titration. Interestingly, the fWW protein containing all four WW domains is capable of binding to Nogo-A with a dissociation constant K_d of 1.68 μM.

To assess their structural properties, far-UV CD spectra were collected for all four isolated WW domains. As seen in Figure 2a, all four WW domains had a positive CD signal at ~230 nm and a negative one at ~208 nm, indicating that all of them possess β-turn/sheet secondary structures, in agreement with the notion that all WW domains adopt a conserved three-stranded β-fold. Interestingly, only WW4 has a positive CD signal at ~200 nm, indicating that WW4 may be the best-structured with tight tertiary packing. To further visualize detailed structural properties of the four isolated WW domains by NMR spectroscopy, they were all ^{15}N isotope-labeled and purified by HPLC for collection of ^{1}H−^{15}N HSQC spectra. Interestingly, as judged from their HSQC spectra, it appears that four WW domains owned very different structural features. WW1 and WW2 were only partially folded which had narrowly dispersed HSQC spectra with only approximately half of the resonance peaks detectable (Figure 3a,b). On the other hand, as seen in Figure 3d, consistent with the CD result, WW4 is the best-folded with uniform HSQC peak intensities in a well-dispersed spectrum (~3 ppm for ^{1}H and 26 ppm for ^{15}N dimensions). With regard to WW3, although it was well folded as evident from its widely dispersed HSQC spectrum, its peak intensities were not uniform and some peaks have minor doublets (Figure 3c), indicating that some regions might undergo intermediate or slow conformational exchanges.

The binding interactions between four WW domains and the Nogo-A(650−666) peptide were assessed by NMR HSQC titrations. Very interestingly, although as shown above, the four WW domains had very different HSQC spectra, addition of Nogo-A(650−666) induced dramatic HSQC peak shifts for all of them (Figure 3), indicating that they were able to bind the Nogo-A(650−666) peptide. In particular, for WW1 and WW2 domains, the introduction of Nogo-A(650−666) resulted in manifestation of HSQC peaks for almost all non-proline residues in well-dispersed HSQC spectra, clearly indicating that upon binding, the WW1 and WW2 domains underwent significant conformational changes from partially folded to well-folded states.

We have compared the HSQC spectrum of the free fWW with the spectrum generated by adding four HSQC spectra of the free WW1−WW4 domains. Interestingly, most HSQC peaks were not superimposable. A similar situation was also observed when the HSQC spectrum of the complexed fWW was compared to that generated by adding four HSQC spectra

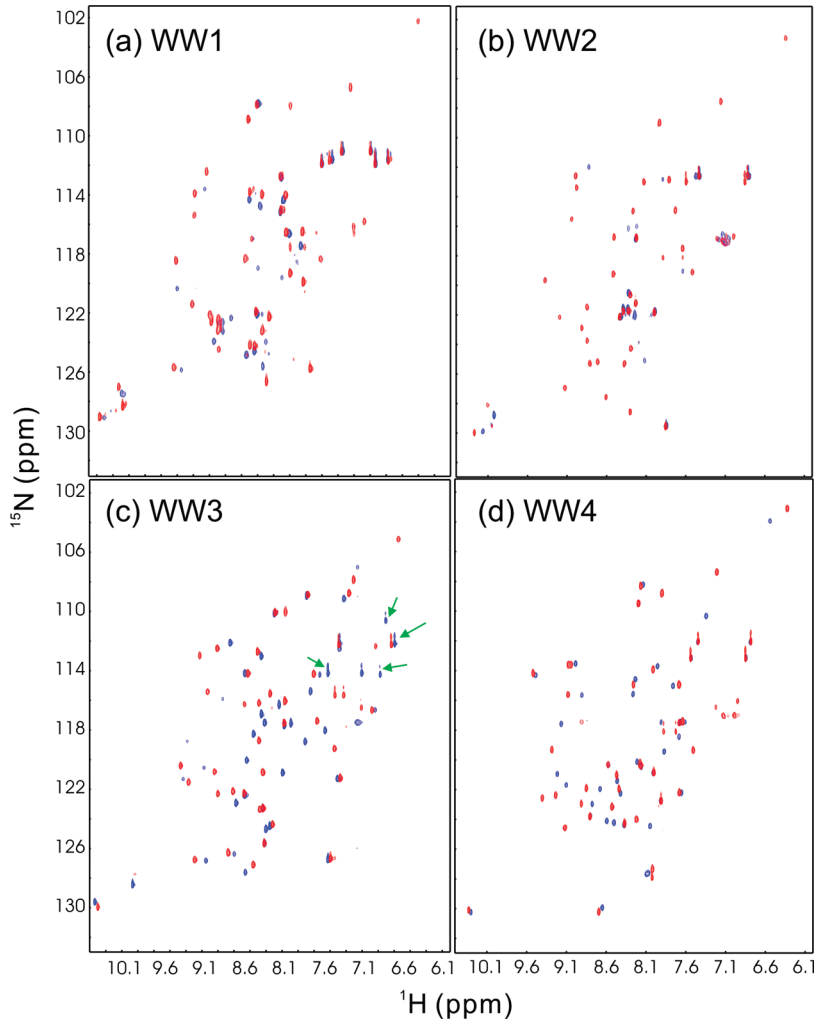

FIGURE 3: Binding of four ^{15}N-labeled WW domains with Nogo-A(650−666). Superimposition of the HSQC spectra of ^{15}N-labeled WW1 (a), WW2 (b), WW3 (c), and WW4 (d) in the absence (blue) and presence (red) of Nogo-A(650−666) at a molar ratio of 1:4 (WW: peptide). All spectra were recorded in a 5 mM phosphate buffer (pH 6.2) at 25 °C on an 800 MHz Bruker NMR spectrometer. The doublets of some HSQC peaks of the complexed WW3 domain are indicated.

of the complexed WW1−WW4 domains. On the other hand, for both the free and complexed states, most HSQC peaks of the summed spectra of the isolated WW1−WW4 domains could be superimposed with those of the spectra collected on the equal molar mixture of four individual WW domains (spectra not shown). This implies that the linker regions in the fWW protein might play a role in constraining or mediating the interactions among four WW domains or/and between four WW domains and Nogo-A peptide.

To quantitatively characterize binding interactions between four WW domains and Nogo-A(650−666), isothermal calorimetric titrations were conducted to determine their thermodynamic binding constants. The raw titration data are shown in Figure 4, while binding parameters obtained by data fitting are presented in Table 1. Very strikingly, although four WW domains possessed very differential structural characteristics, they had very similar binding affinities for the Nogo-A(650−666) peptide, with dissociation constants of 1.03 μM for WW1, 3.85 μM for WW2, 1.85 μM for WW3, and 1.50 μM for WW4. Judging from the previous reports (*35*−*38*), the binding interactions between the WWP1 WW domains and Nogo-A can be ranked within a high-affinity category among previously documented WW−ligand interactions. Interestingly, as seen in Table 1, the thermodynamic parameters for the fWW protein are not the averages of those of four individual WW1−WW4 domains. This implies that the interaction of fWW with Nogo-A might be slightly different from those of four isolated WW domains with Nogo-A, completely consistent with the NMR results described above.

NMR Characterization of Binding Interactions. The detailed binding of Nogo-A(650−666) to fWW and four WW domains was also characterized by monitoring the HSQC peak shifts of the ^{15}N-labeled Nogo-A(650−666) peptide induced by a gradual addition of different WW domains. Unfortunately, due to the poor solubility of the fWW protein, its interaction with the ^{15}N-labeled Nogo-A(650−666) peptide could not be investigated in detail. On the other hand, however, four WW domains induced very similar shift patterns for the HSQC peaks of Nogo-A(650−666), indicating that they interacted with Nogo-A in a similar manner. As a consequence, extensive NMR studies were performed on the interaction between the best-folded WW4 domain and the Nogo-A(650−666) peptide. As seen in Figure 5a, upon addition of the WW4 domain at a 4-fold excess, the HSQC peaks of the characteristic Tyr659 residue with its neighboring residue Glu660 totally disappeared, indicating the binding would induce dramatic conformational exchanges on the

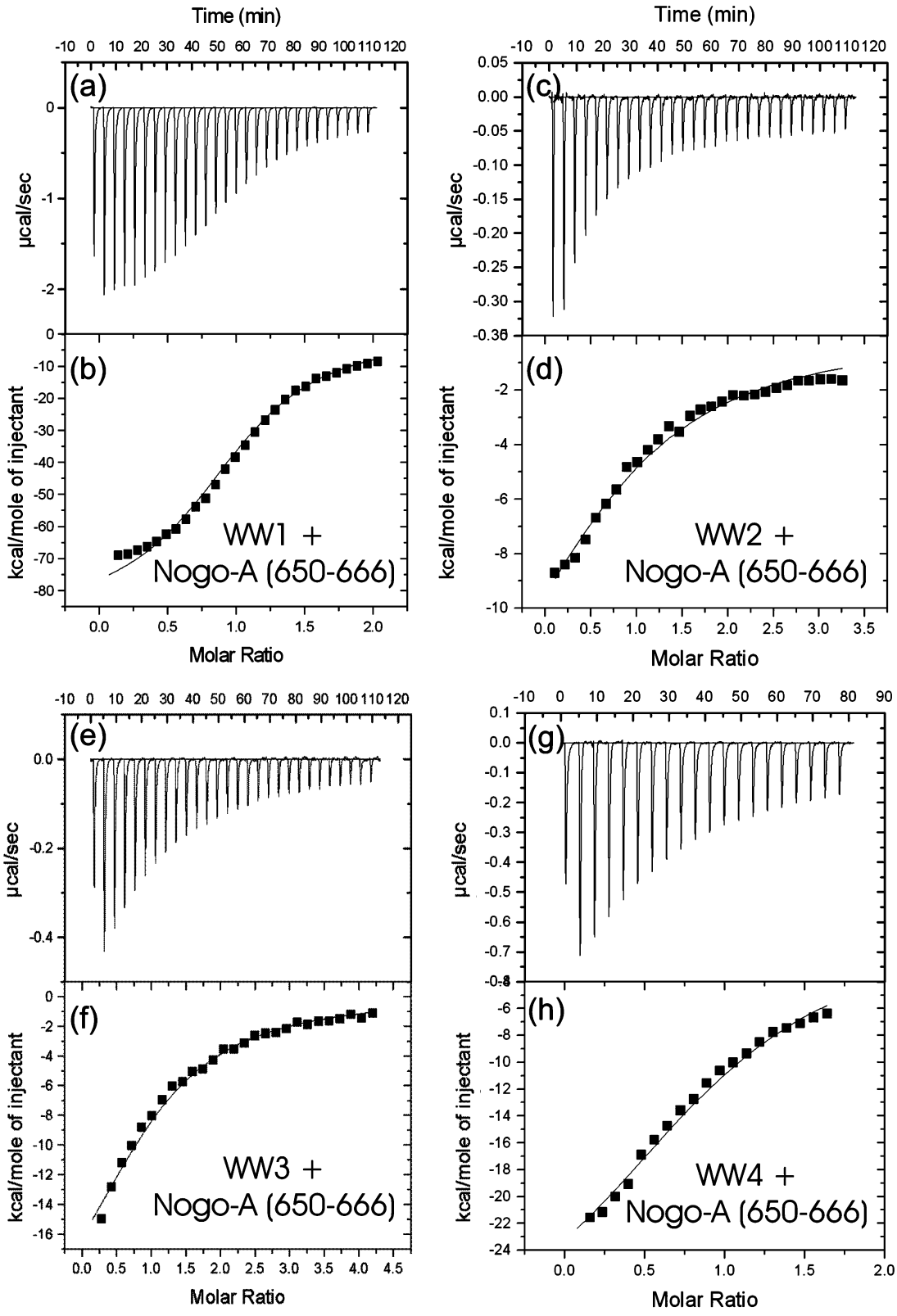

FIGURE 4: ITC characterization. ITC titration profiles of the binding reactions of the WW1 (a), WW2 (c), WW3 (e), and WW4 (g) domains with Nogo-A(650−666). Integrated values for reaction heats with subtraction of the corresponding blank results normalized by the amount of ligand injected vs the Nogo-A:WW1 (b), Nogo-A:WW2 (d), Nogo-A:WW3 (f), and Nogo-A:WW4 (h) molar ratio. The detailed conditions and settings of the ITC experiments are presented in Materials and Methods and Table 1.

microsecond to millisecond time scale (*18, 20, 25*). It is worth noting that residues Glu652, Glu654, and Asn655 N-terminal to the PPPY motif also underwent significant shifts, indicating that these residues might also play an important role in mediating the binding affinity and specificity.

Three-Dimensional Structure and Binding Interface of the WW4 Domain. It would be most relevant if the three-dimensional structure of fWW containing all four WWP1 WW domains could be determined in complex with the Nogo-A peptide. However, as shown above, the poor quality

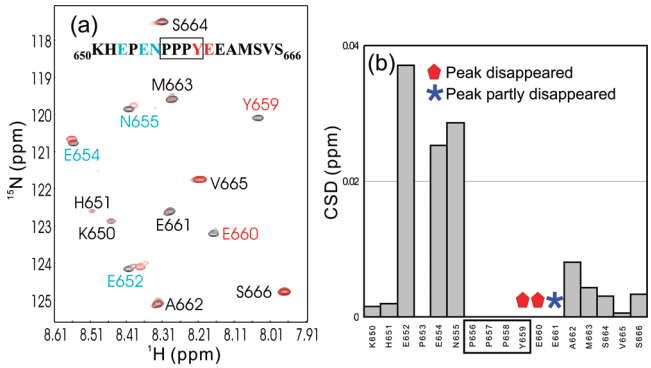

FIGURE 5: Binding of ^{15}N-labeled Nogo-A(650−666) with the WW4 domain. (a) Superimposition of the HSQC spectra of the ^{15}N-labeled Nogo-A(650−666) peptide in the absence (black) and presence (red) of the WW4 domain at a 1:4 peptide:WW4 molar ratio. All spectra were recorded in a 5 mM phosphate buffer (pH 6.2) at 25 °C on an 800 MHz NMR spectrometer. The sequential assignments of Nogo-A(650−666) were made by analyzing heteronuclear HSQC-TOCSY and HSQC-NOESY spectra. The sequence of Nogo-A(650−666) was included, and the two residues (Tyr659 and Glu660) with HSQC peaks that completely disappeared upon binding are labeled in red. Residues Glu652, Glu654, and Asn655 with significant peak shifts upon binding are labeled in cyan. (b) Residue-specific chemical shift difference (CSD) of Nogo-A(650−666) induced by binding to the WW4 domain. The bar values were calculated from the shifts observed in Figure 5a using the formula described in Materials and Methods. The characteristic WW domain binding PPPY motif in Nogo-A(650−666) is boxed.

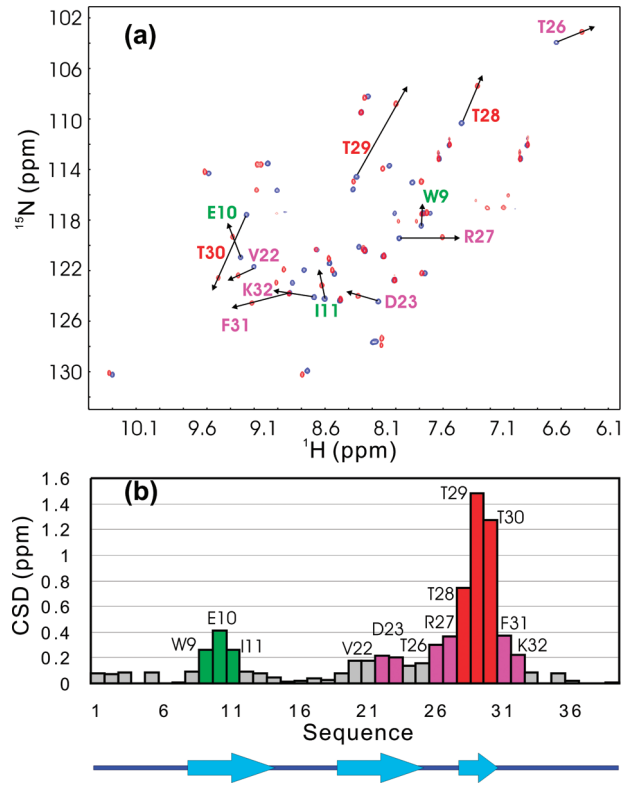

FIGURE 6: Binding of the ^{15}N-labeled WW4 domain with Nogo-A(650−666). (a) Superimposition of the HSQC spectra of the ^{15}N-labeled WW4 domain in the absence (blue) and presence (red) of Nogo-A(650−666) at a 1:4 WW4:peptide molar ratio. All spectra were acquired in 5 mM phosphate buffer (pH 6.2) at 25 °C on an 800 MHz NMR spectrometer. The sequential assignments of WW4 were made by analyzing heteronuclear HSQC-TOCSY and HSQC-NOESY spectra. The residues with significant peak shifts upon binding are labeled in the spectra. (b) Residue-specific chemical shift difference (CSD) of WW4 induced by binding to Nogo-A(650−666). The bar values were calculated from the shifts observed in Figure 7A using the formula described in Materials and Methods. Red was used for coloring residues with changes larger than 0.6, pink for residues with changes larger than 0.2 but smaller than 0.6 if on the third β-strand, and green for residues on the first β-strand.

of the HSQC spectrum and low solubility of the fWW protein made the detailed NMR study impossible. On the other hand, WW1 and WW2 are only partially folded while WW3 also undergoes extensive conformational exchanges and is, thus, not suitable for structure determination in the free state. We have also attempted to determine the WW1 structure in complex with the Nogo-A peptide but failed because many Cα and Cβ resonance peaks were undetectable even in the triple-resonance HNCACB and CBCA(CO)NH experiments. Furthermore, as shown in Figure 5a, when Nogo-A binds to isolated WW domains, the HSQC peaks of the key Nogo-A residues completely disappeared, suggesting that it was impossible to determine the complex structure by identifying intermolecular NOE connectivities. Therefore, in this study, we decided to determine the solution structure of the best-folded WW4 domain in the free state and subsequently derived its complex model by the well-established HADDOCK procedure which makes use of the NMR HSQC titration data.

Figure 6a shows the ^{1}H−^{15}N HSQC spectra of the WW4 domain in the absence and presence of Nogo-A(650−666) at a 1:4 WW4:peptide ratio, while Figure 6b presents the residue-specific chemical shift difference (CSD). Interestingly, the significantly perturbed residues (with a shift index of >0.2 ppm) were located over two regions, one over Trp9-Glu10-Ile11 and another over Thr28-Thr29-Thr30. This result is in agreement with the notion that for the WW domains, two discrete regions were mainly responsible for binding to the ligand, one centralized around the first Trp residue and another around the second Trp residue. However, it is very interesting to note that in WW4, the most-perturbed residues were centralized around Thr28-Thr29-Thr30 but not Phe31 corresponding to the second Trp in other WW domains.

By using experimental NMR distance and dihedral angle constraints, the three-dimensional structure of the WW4 domain was determined. Figure 7a shows the 10 solution structures with the lowest target functions, while Table 2 presents their structural statistics. As seen in Figure 7a, the WW4 domain adopts an antiparallel three-stranded β-sheet fold common to all WW domains (*35*−*37*), with the first β-strand over residues Gly8−Tyr13, the second over Arg19−His24, and the third over Thr28-Phe31. Interestingly, in the WWP1 WW4 domain there is a short C-terminal 3_{10}-helix formed over residues Pro34−Asn36 which is not conserved in the classic WW fold. In the 10 WW4 solution structures, the secondary structure regions are well-defined, with rms deviations of 1.37 Å for all atoms, 1.12 Å for the heavy atoms, and 0.25 Å for the backbone atoms.

On the basis of the HSQC titration data for both the WW4 domain and the Nogo-A peptide, we have constructed the model of the WW4 domain in complex with the Nogo-A peptide by the well-established HADDOCK 2.0 program with the best structural solution shown in panels b and c of Figure 7. As seen in panels a and b of Figure 7, the Nogo-A peptide binds to the WWP1 WW4 domain in a manner very

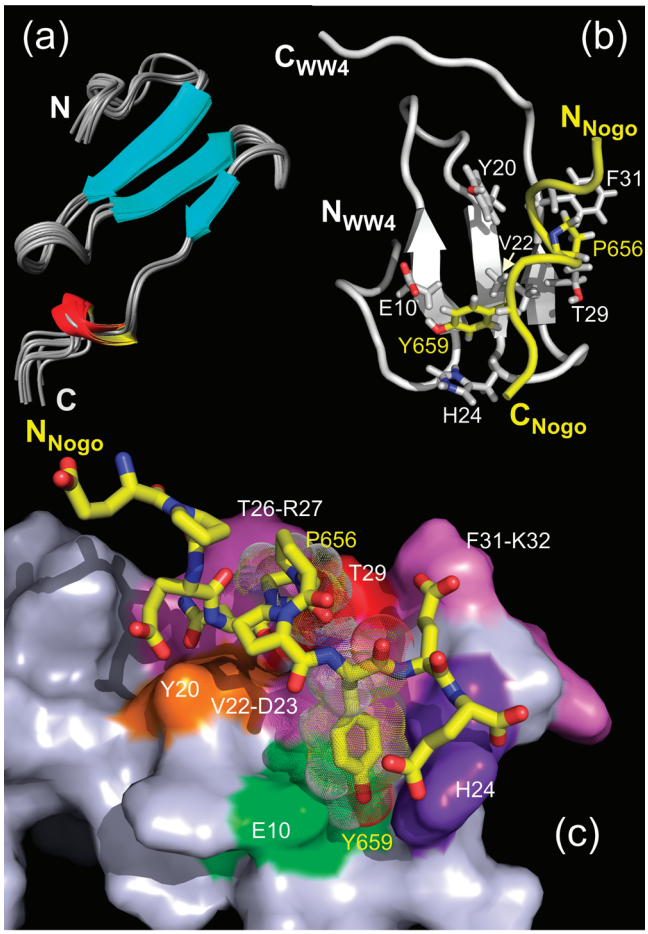

FIGURE 7: Structures of the free and complexed WW4 domains. (a) Superimposition of the 10 selected NMR structures of the WW4 domain having the lowest target functions in ribbon mode. (b) Best docking solution of the WW4 domain (gray) in complex with the Nogo-A peptide (yellow). The side chains of the binding-important residues are displayed as sticks and labeled for both the WW4 domain and Nogo-A peptide. (c) Surface representation of the WW4 domain in complex with the Nogo-A peptide in stick mode. The binding-perturbed WW4 residues are colored as in Figure 6b. Additional residue His24 is colored purple and Tyr20 brown.

similar to those previously reported for other WW−PPxY complexes (*39*−*44*). Briefly, the major WW4 residues in contact with the Nogo-A peptides include two aromatic residues (Tyr20 and Phe31), Val22, His24, and Thr29 which are highly conserved and thus thought to be common residues critical for ligand binding. On the other hand, residue Glu10 located in the first β-strand also has a close contact with the Tyr659 side chain. Interestingly, in WW domains such as from Yap and Rsp proteins, the position corresponding to Glu10 is occupied by the negatively charged Glu residue. By contrast, in some other WW domains from Ykb2, Db10, and Yfx1 proteins, this position resides in a positively charged Lys residue. As seen in Figure 6, upon binding to Nogo-A, Glu10 in the WW4 domain is also significantly perturbed, implying that it may play an important role in the binding of the WWP1 WW4 domain to Nogo-A. The result that the mutation of Tyr659 completely abolished the binding ability of the Nogo-A peptide strongly highlights the critical role of Tyr659 in binding with the WWP1 WW4 domain. Indeed, as seen in Figure 7c, the Tyr659 side chain deeply inserts into a pocket formed by residues Glu10 and His24, thus explaining why WW4 residue Glu10 was significantly perturbed by binding to the Nogo-A peptide (Figure 6). Furthermore, in the complex model, Nogo-A residue Pro656 has a close contact with WW4 residue Thr29, thus rationalizing the observation that upon binding to the Nogo-A peptide, the residues centralizing Thr28-Thr29-Thr30 were significantly perturbed (Figure 6).

DISCUSSION

Nogo-A is a multifunctional protein which has been implicated in a variety of diverse and important biological processes, including inhibition of neural regeneration (*8*), participation in ER shaping (*11*), and stabilization of neuromuscular junction (*12*). In particular, changes in the intracellular Nogo-A protein level have been directly associated with stroke (*45*) as well as other neurodegenerative diseases such as amyotrophic lateral sclerosis (ALS) (*46, 47*) and Alzheimer's disease (*48*). These observations clearly indicate that the Nogo-A protein level represents a critical factor in regulation of its functions. However, so far how the Nogo-A protein level is regulated in cells remains unknown. On the other hand, Nogo-A is extensively believed to interact with many other proteins, and consequently, identification of such novel binding partners holds key implications in understanding the functional roles of Nogo-A as well as designing molecules of therapeutic interest.

In this study, we first successfully identified WWP1 to be a novel binding partner of Nogo-A. In particular, our results demonstrate that WWP1 forms a complex with the endogenous Nogo-A both in vitro and in vivo. WWP1 belongs to the E3 ubiquitin ligase family which is the critical component that provides specificity to the Ub system. More specifically, WWP1 utilizes its WW modular domains to specifically bind to the PPxY motif in the substrate and consequently promotes ligation of ubiquitin to the substrate (*49*−*54*). Currently, we have obtained the in vivo results revealing that WWP1 indeed binds Nogo-A to promote Nogo-A ubiquitination, thus regulating the Nogo-A protein level (to be published elsewhere). Given the critical role of the Nogo-A protein level in various human diseases, the Nogo-A−WWP1 interaction interface may represent a promising target for developing molecules of medical interest.

So far, no structural study has been reported for the WWP1 WW domains. Given the crucial role of the interaction between the WWP1 WW domains and PPxY motif in its substrates (*49*−*54*), we further conducted extensive investigations on all four WWP1 WW domains as well as their interactions with the Nogo-A(650−666) peptide carrying the only Nogo-A PPxY motif by using ITC, CD, and NMR spectroscopy. The results show that despite containing a large unstructured region in the 186-residue fWW protein consisting of all four WW domains, it is able to bind to the Nogo-A(650−666) peptide with a high affinity, with a K_d of 1.68 μM. On the other hand, surprisingly, the CD and NMR characterization reveals that four isolated WWP1 WW domains have differential structural properties. While the fourth WW domain is well-folded, the first and second WW domains undergo extensive conformational exchanges on the microsecond to millisecond time scale, likely due to a slight unfolding as we previously discovered (*55, 56*) or/and a slight dynamic aggregation, which causes many HSQC peaks to be undetectable. Nevertheless, as revealed by ITC measure-

ments, all four WWP1 WW domains are capable of binding to Nogo-A(650−666) with similar affinities, with K_d values ranging from 1.03 to 3.85 μM, which can be ranked within a high-affinity category among previously documented WW−ligand interactions (*35*−*38*). Very interestingly, as shown by NMR characterization, the partially folded WW1 and WW2 domains suddenly undergo significant conformational transitions to become well-structured upon binding to Nogo-A(650−666). This phenomenon is rarely observed for the native WW domains, and previously, only one engineered Trp17-to-Phe mutant of the YAP WW domain was found to be partially unfolded in the free state but became structured upon binding to the PPxY ligand (*43*).

Further structure determination of the best-folded WW4 domain by NMR spectroscopy shows that it adopts a common WW fold with an antiparallel three-stranded β-sheet, with an additional C-terminal 3_{10}-helix. Detailed HSQC titrations indicate that the Nogo-A binding interface of the WW4 domain is mostly constituted by residues centralized over the Thr28-Thr29-Thr30 sequence on the third β-strand and over the Trp9-Glu10-Ile11 sequence on the first strand. Furthermore, the complex model generated from molecular docking suggests that the Nogo-A peptide binds to the WW4 domain in a mode very similar to those previously reported. More importantly, the complex model rationalizes the HSQC titration results as well as the mutation result that Tyr665 of Nogo-A(650−666) is absolutely indispensable for the binding to the WW4 domain. Recently, we have demonstrated that the whole 1016-residue N-terminus of human Nogo-A was intrinsically unstructured (*17*). Therefore, in vivo this WW-binding motif of Nogo-A might be already accessible to WWP1 without needing to be further unfolded.

In conclusion, we have identified WWP1, an E3 ubiquitin ligase, as a novel binding partner for Nogo-A which may regulate the Nogo-A protein level in vivo. With consideration that the protein level of Nogo-A is a key factor regulating its functions, and in particular correlated with human diseases, the interaction interface between the WWP1 WW domains and the Nogo-A PPPY motif might represent a promising target for design of molecules of significant medical interest. In this regard, this study also provides rationales as well as a template Nogo-A(650−666) for further drug design.

ACKNOWLEDGMENT

We thank Dr. Alexandre M. J. J. Bonvin at Utrecht University (Utrecht, The Netherlands) for the HADDOCK software and suggestions on the docking setup.

REFERENCES

1. Oertle, T., Huber, C., van der Putten, H., and Schwab, M. E. (2003) Genomic structure and functional characterisation of the promoters of human and mouse nogo/rtn4. *J. Mol. Biol. 325*, 299–323.
2. Dodd, D. A., Niederoest, B., Bloechlinger, S., Dupuis, L., Loeffler, J., and Schwab, M. E. (2005) Nogo-A, -B, and -C are found on the cell surface and interact together in many different cell types. *J. Biol. Chem. 280*, 12494–12502.
3. Chen, M. S., Huber, A. B., van der Haar, M. E., Frank, M., Schnell, L., Spillmann, A. A., Christ, F., and Schwab, M. E. (2000) Nogo-A is a myelin-associated neurite outgrowth inhibitor and an antigen for monoclonal antibody IN-1. *Nature 403*, 369–370.
4. GrandPre, T., Nakamura, F., Vartanian, T., and Strittmatter, S. M. (2000) Identification of the Nogo inhibitor of axon regeneration as a Reticulon protein. *Nature 403*, 439–444.
5. Prinjha, R., Moore, S. E., Vinson, M., Blake, S., Morrow, R., Christie, G., Michalovich, D., Simmons, D. L., and Walsh, F. S. (2000) Inhibitor of neurite outgrowth in humans. *Nature 403*, 383–384.
6. Hunt, D., Coffin, R. S., Prinjha, R. K., Campbell, G., and Andersonb, P. N. (2003) Nogo-A expression in the intact and injured nervous system. *Mol. Cell. Neurosci. 24*, 1083–1102.
7. Oertle, T., van der Haar, M. E., Bandtlow, C. E., Robeva, A., Burfeind, P., Buss, A., Huber, A. B., Simonen, M., Schnell, L., Brosamle, C., Kaupmann, K., Vallon, R., and Schwab, M. E. (2003) Nogo-A inhibits neurite outgrowth and cell spreading with three discrete regions. *J. Neurosci. 23*, 5393–5406.
8. Schwab, M. E. (2004) Nogo and axon regeneration. *Curr. Opin. Neurobiol. 14*, 118–124.
9. Liebscher, T., Schnell, L., Schnell, D., Scholl, J., Schneider, R., Gullo, M., Fouad, K., Mir, A., Rausch, M., Kindler, D., Hamers, F. P., and Schwab, M. E. (2005) Nogo-A antibody improves regeneration and locomotion of spinal cord-injured rats. *Ann. Neurol. 58*, 706–719.
10. Freund, P., Schnidlin, E., Wannier, T., Bloch, J., Mir, A., Schwab, M. E., and Rouiller, E. M. (2006) Nogo-A-specific antibody treatment enhances sprouting and functional recovery after cervical lesion in adult primates. *Nat. Med. 12*, 790–792.
11. Voeltz, G. K., Prinz, W. A., Shibata, Y., Rist, J. M., and Rapoport, T. A. (2006) A class of membrane proteins shaping the tubular endoplasmic reticulum. *Cell 124*, 573–586.
12. Jokic, N., Gonzalez de Aguilar, J. L., Dimou, L., Lin, S., Fergani, A., Ruegg, M. A., Schwab, M. E., Dupuis, L., and Loeffler, J. P. (2006) The neurite outgrowth inhibitor Nogo-A promotes denervation in an amyotrophic lateral sclerosis model. *EMBO Rep. 7*, 1162–1167.
13. Fournier, A. E., GrandPre, T., and Strittmatter, S. M. (2001) Identification of a receptor mediating Nogo-66 inhibition of axonal regeneration. *Nature 409*, 341–346.
14. Li, M., Shi, J., Wei, Z., Teng, F. Y., Tang, B. L., and Song, J. (2004) Structural characterization of the human Nogo-A functional domains. Solution structure of Nogo-40, a Nogo-66 receptor antagonist enhancing injured spinal cord regeneration. *Eur. J. Biochem. 271*, 3512–3522.
15. Li, M., Liu, J., and Song, J. (2006) Nogo goes in the pure water: Solution structure of Nogo-60 and design of the structured and buffer-soluble Nogo-54 for enhancing CNS regeneration. *Protein Sci. 15*, 1835–1841.
16. Niedero, B., Oertle, T., Fritsche, J., McKinney, R. A., and Bandtlow, C. E. (2002) Nogo-A and myelin-associated glycoprotein mediate neurite growth inhibition by antagonistic regulation of RhoA and Rac1. *J. Neurosci. 22*, 10368–10376.
17. Li, M., and Song, J. (2007) The N- and C-termini of the human Nogo molecules are intrinsically unstructured: Bioinformatics, CD, NMR characterization, and functional implications. *Proteins 68*, 100–108.
18. Liu, J., Li, M., Ran, X., Fan, J. S., and Song, J. (2006) Structural insight into the binding diversity between the human Nck2 SH3 domains and proline-rich proteins. *Biochemistry 45*, 7171–7184.
19. Komuro, A., Imamura, T., Saitoh, M., Yoshida, Y., Yamori, T., Miyazono, K., and Miyazawa, K. (2004) Negative regulation of transforming growth factor-β (TGF-β) signaling by WW domain-containing protein 1 (WWP1). *Oncogene 23*, 6914–6923.
20. Ran, X., Qin, H., Liu, J., Fan, J. S., Shi, J., and Song, J. (2008) NMR structure and dynamics of human ephrin-B2 ectodomain: The functionally critical C-D and G-H loops are highly dynamic in solution. *Proteins 72*, 1019–1029.
21. Sattler, M., Schleucher, J., and Griesinger, C. (1999) Heteronuclear multidimensional NMR experiments for the structure determination of proteins in solution employing pulsed field gradients. *Prog. NMR Spectrosc. 34*, 93–158.
22. Ran, X., and Song, J. (2005) Structural insight into the binding diversity between the Tyr-phosphorylated human ephrinBs and Nck2 SH2 domain. *J. Biol. Chem. 280*, 19205–19212.
23. Delaglio, F., Grzesiek, S., Vuister, G. W., Zhu, G., Pfeifer, J., and Bax, A. (1995) A multidimensional spectral processing system based on UNIX pipes. *J. Biomol. NMR 6*, 277–293.
24. Johnson, B. A., and Blevins, R. A. (1994) NMRView: A computer program for the visualization and analysis of NMR data. *J. Biomol. NMR 4*, 603–614.

25. Qin, H., Shi, J., Noberini, R., Pasquale, E. B., and Song, J. (2008) Crystal structure and NMR binding reveal that two small molecule antagonists target the high-affinity ephrin-binding channel of the EphA4 receptor. *J. Biol. Chem. 283*, 29473–29484.
26. Guntert, P. (2004) Automated NMR structure calculation with CYANA. *Methods Mol. Biol. 278*, 353–378.
27. Cornilescu, G., Delaglio, F., and Bax, A. (1999) Protein backbone angle restraints from searching a database for chemical shift and sequence homology. *J. Biomol. NMR 13*, 289–302.
28. Laskowski, R. A., Rullmannn, J. A., MacArthur, M. W., Kaptein, R., and Thornton, J. M. (1996) AQUA and PROCHECK-NMR: Program for checking the quality of protein structures solved by NMR. *J. Biomol. NMR 8*, 477–486.
29. Koradi, R., Billeter, M., and Wuthrich, K. (1996) MOLMOL: A program for display and analysis of macromolecular structures. *J. Mol. Graphics 14*, 51–55.
30. Dominguez, C., Boelens, R., and Bonvin, A. M. (2003) HADDOCK: A protein-protein docking approach based on biochemical or biophysical information. *J. Am. Chem. Soc. 125* (7), 1731–1737.
31. Cesareni, G., Castagnoli, L., and Cestra, G. (1999) Phage displayed peptide libraries. *Comb. Chem. High Throughput Screening 2*, 1–17.
32. Castagnoli, L., Zucconi, A., Quondam, M., Rossi, M., Vaccaro, P., Panni, S., Paoluzi, S., Santonico, E., Dente, L., and Cesareni, G. (2001) Alternative bacteriophage display systems. *Comb. Chem. High Throughput Screening 4*, 121–133.
33. Venyaminov, S. Y., and Yang, J. T. (1996) Determination of protein secondary structure. In *Circular Dichroism and the Conformational Analysis of Biomolecules* (Fasman, G. D., Ed.) pp 69−107, Plenum Press, New York.
34. Liu, J., and Song, J. (2008) NMR Evidence for Forming Highly-Populated Helical Conformations in the Partially-Folded hNck2 SH3 Domain. *Biophys. J.* , PMID 18599634.
35. Macias, M. J., Wiesner, S., and Sudol, M. (2002) WW and SH3 domains, two different scaffolds to recognize proline-rich ligands. *FEBS Lett. 513*, 30–37.
36. Ilsley, J. L., Sudol, M., and Winder, S. J. (2002) The WW domain: Linking cell signalling to the membrane cytoskeleton. *Cell Signalling 14*, 183–189.
37. Einbond, A., and Sudol, M. (1996) Towards prediction of cognate complexes between the WW domain and proline-rich ligands. *FEBS Lett. 384*, 1–8.
38. Otte, L., Wiedemann, U., Schlegel, B., Pires, J. R., Beyermann, M., Schmieder, P., Krause, G., Volkmer-Engert, R., Schneider-Mergener, J., and Oschkinat, H. (2003) WW domain sequence activity relationships identified using ligand recognition propensities of 42 WW domains. *Protein Sci. 12*, 491–500.
39. Macias, M. J., Hyvönen, M., Baraldi, E., Schultz, J., Sudol, M., Saraste, M., and Oschkinat, H. (1996) Structure of the WW domain of a kinase-associated protein complexed with a proline-rich peptide. *Nature 382*, 646–649.
40. Pires, J. R., Taha-Nejad, F., Toepert, F., Ast, T., Hoffmüller, U., Schneider-Mergener, J., Kühne, R., Macias, M. J., and Oschkinat, H. (2001) Solution structures of the YAP65 WW domain and the variant L30 K in complex with the peptides GTPPPPYTVG, N-(n-octyl)-GPPPY and PLPPY and the application of peptide libraries reveal a minimal binding epitope. *J. Mol. Biol. 314*, 1147–1156.
41. Kanelis, V., Bruce, M. C., Skrynnikov, N. R., Rotin, D., and Forman-Kay, J. D. (2006) Structural determinants for high-affinity binding in a Nedd4 WW3* domain-Comm PY motif complex. *Structure 14*, 543–553.
42. Chong, P. A., Lin, H., Wrana, J. L., and Forman-Kay, J. D. (2006) An expanded WW domain recognition motif revealed by the interaction between Smad7 and the E3 ubiquitin ligase Smurf2. *J. Biol. Chem. 281*, 17069–17075.
43. Koepf, E. K., Petrassi, H. M., Ratnaswamy, G., Huff, M. E., Sudol, M., and Kelly, J. W. (1999) Characterization of the structure and function of W → F WW domain variants: Identification of a natively unfolded protein that folds upon ligand binding. *Biochemistry 38*, 14338–14351.
44. Jäger, M., Zhang, Y., Bieschke, J., Nguyen, H., Dendle, M., Bowman, M. E., Noel, J. P., Gruebele, M., and Kelly, J. W. (2006) Structure-function-folding relationship in a WW domain. *Proc. Natl. Acad. Sci. U.S.A. 103*, 10648–10653.
45. Li, S., and Carmichael, S. T. (2006) Growth-associated gene and protein expression in the region of axonal sprouting in the aged brain after stroke. *Neurobiol. Dis. 23*, 362–373.
46. Jokic, N., Gonzalez de Aguilar, J. L., Pradat, P. F., Dupuis, L., Echaniz-Laguna, A., Muller, A., Dubourg, O., Seilhean, D., Hauw, J. J., Loeffler, J. P., and Meininger, V. (2005) Nogo expression in muscle correlates with amyotrophic lateral sclerosis severity. *Ann. Neurol. 57*, 553–556.
47. Pradat, P. F., Bruneteau, G., Gonzalez de Aguilar, J. L., Dupuis, L., Jokic, N., Salachas, F., Le Forestier, N., Echaniz-Laguna, A., Dubourg, O., Hauw, J. J., Tranchant, C., Loeffler, J. P., and Meininger, V. (2007) Muscle Nogo-A expression is a prognostic marker in lower motor neuron syndromes. *Ann. Neurol. 62*, 15–20.
48. Gil, V., Nicolas, O., Mingorance, A., Urena, J. M., Tang, B. L., Hirata, T., Saez-Valero, J., Ferrer, I., Soriano, E., and del Rio, J. A. (2006) Nogo-A expression in the human hippocampus in normal aging and in Alzheimer disease. *J. Neuropathol. Exp. Neurol. 65*, 433–444.
49. Pickart, C. M. (2001) Mechanisms underlying ubiquitination. *Annu. Rev. Biochem. 70*, 503–533.
50. Harvey, K. F., and Kumar, S. (1999) Nedd4-like proteins: An emerging family of ubiquitin-protein ligases implicated in diverse cellular functions. *Trends Cell Biol. 9*, 166–169.
51. Ingham, R. J., Gish, G., and Pawson, T. (2004) The Nedd4 family of E3 ubiquitin ligases: Functional diversity within a common modular architecture. *Oncogene 23*, 1972–1984.
52. Shearwin-Whyatt, L., Dalton, H. E., Foot, N., and Kumar, S. (2006) Regulation of functional diversity within the Nedd4 family by accessory and adaptor proteins. *BioEssays 28*, 617–628.
53. Chen, C., and Matesic, L. E. (2007) The Nedd4-like family of E3 ubiquitin ligases and cancer. *Cancer Metastasis Rev. 26*, 587–604.
54. Bernassola, F., Karin, M., Ciechanover, A., and Melino, G. (2008) The HECT family of E3 ubiquitin ligases: Multiple players in cancer development. *Cancer Cell 14*, 10–21.
55. Song, J., Jamin, N., Gilquin, B., Vita, C., and Menez, A. (1999) A gradual disruption of tight side-chain packing: 2D ^{1}H-NMR characterization of acid-induced unfolding of CHABII. *Nat. Struct. Biol. 6*, 129–134.
56. Wei, Z., and Song, J. (2005) Molecular mechanism underlying the thermal stability and pH-induced unfolding of CHABII. *J. Mol. Biol. 348*, 205–218.

BI8017976